CHAPTER

Cohesive Zone Model 9

To a beginner, the most difficult concept to accept in the linear elastic fracture mechanics (LEFM) is the fact that stresses at the crack tip are infinitely large, or singular. This stress singularity results from the linear elastic continuum representation of materials and the assumption of a perfectly sharp crack. Since stress singularity contradicts our intuition about failure of materials, there have been efforts in introducing ways to remove the stress singularity at the crack tip. Adopting inelastic behavior in solids is a natural extension of the LEFM to avoid stress singularity. Irwin's plastic zone adjustment approach as discussed in Chapter 6 belongs to this category. However, such an approach often goes back to using the parameters employed by the LEFM such as stress intensity factor.

A somewhat different approach toward the same objective is the cohesive zone model, which adds a zone of vanishing thickness ahead of the crack tip with the intention of describing more realistically the fracture process without the use of stress singularity. The cohesive zone is idealized as two cohesive surfaces, which are held together by a cohesive traction. The material failure is characterized by the complete separation of the cohesive surfaces and the separation process is described by a cohesive law that relates the cohesive traction and the relative displacement of the cohesive surfaces. Hence, a physical crack extension occurs when the separation displacement at the tail of the cohesive zone (physical crack tip) reaches a critical value. One of the key advantages offered by the cohesive zone model is that it has an intrinsic fracture energy dissipation mechanism in contrast to the classical continuum based fracture mechanics for which such a mechanism is absent.

9.1 THE BARENBLATT MODEL

Barenblatt [9-1] proposed a cohesive zone concept to study the fracture of brittle materials, aiming to introduce a separation mechanism at the atomic level to describe the actual separation of materials, and to eliminate the crack tip stress singularity. Barenblatt believed that the crack surfaces at the tip region are so close that they can be treated as two atomic layers held by the atomic bonding forces, as shown in

Fracture Mechanics. DOI: 10.1016/B978-0-12-385001-0.00009-2

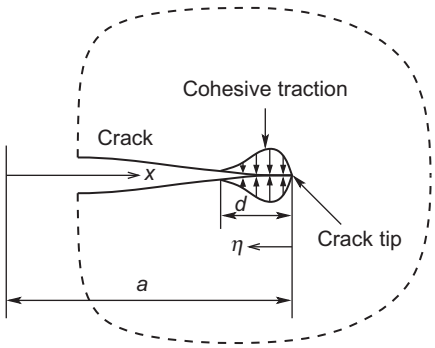

FIGURE 9.1

A Barenblatt cohesive zone near a crack tip.

Figure 9.1. The Barenblatt theory of brittle fracture is based on the following three basic hypotheses:

1. There exists a cohesive zone near the crack tip where the upper and lower crack faces are held by the so-called cohesive traction, which has a magnitude on the order of up to the theoretical strength of the solid. The size of the cohesive zone is much smaller than the crack length.
2. The size of the cohesive zone, and the distribution and magnitude of the cohesive traction at the onset of crack growth are independent of crack geometries and external loads.
3. Stresses are finite everywhere including the crack tip, that is, no stress singularity exists at the crack tip. The first two assumptions were explicitly described in the original paper of Barenblatt [9-1]. The third assumption was actually used in the derivation. Note that the cohesive zone in the Barenblatt model is actually part of the crack.

Now we use a Mode I crack in an infinite elastic solid as an example to illustrate the Barenblatt theory for brittle solids. Consider a through crack of length $2a$ in a two-dimensional infinite elastic solid subjected to uniform tension, σ_∞, at infinity. According to the first assumption of the Barenblatt theory, a small part of the crack faces, called the cohesive zone, near each tip is acted on by the cohesive traction, as shown in Figure 9.1. The size of the cohesive zone, d, is much smaller than the crack length, that is, $d/a << 1$. The distribution of the cohesive traction is represented by

$$\sigma = g(x), \quad a - d \le |x| \le a$$

where σ is the cohesive traction.

In the Barenblatt model, the bulk material is still regarded as an elastic continuum. Consequently, the superposition method can be used to treat the problem. According

to LEFM, the normal stress at the crack line near the crack tip due to the remote tension is given by (see Eqs. (3.41) and (3.44) in Chapter 3)

$$\sigma_{yy}^{(1)} = \frac{K_I}{\sqrt{2\pi(x-a)}}, \quad x > a \tag{9.1}$$

where $K_I = \sigma_\infty \sqrt{\pi a}$ is the stress intensity factor. Meanwhile, the normal stress ahead of the crack tip induced by the cohesive traction $g(x)$ can be written as

$$\sigma_{yy}^{(2)} = \frac{-B}{\sqrt{2\pi(x-a)}}, \quad x > a \tag{9.2}$$

where B may be obtained using the stress intensity factor formula for concentrated forces and the superposition method described in Eq. (3.79) in Chapter 3:

$$B = 2\sqrt{\frac{a}{\pi}} \int_{a-d}^{a} \frac{g(\xi)d\xi}{\sqrt{a^2 - \xi^2}}$$

Here B is actually $-K_I$ in Eq. (3.79) and $g(\xi)$ is symmetric. By using the first assumption $d/a << 1$, this equation becomes

$$B = \sqrt{\frac{2}{\pi}} \int_0^d \frac{g(\eta)d\eta}{\sqrt{\eta}} \tag{9.3}$$

where $\eta = a - \xi$. The total normal stress near the crack tip thus becomes

$$\sigma_{yy} = \sigma_{yy}^{(1)} + \sigma_{yy}^{(2)} = \frac{K_I - B}{\sqrt{2\pi(x-a)}}, \quad x > a \tag{9.4}$$

The third assumption in the Barenblatt theory now requires the removal of the stress singularity at the crack tip. This is fulfilled by requiring that

$$K_I - B = 0 \tag{9.5}$$

that is, B always equals K_I.

Up to this point, we have said nothing about the magnitude and the distribution of the cohesive traction, and the size of the cohesive zone except that it is small. Because K_I increases with the applied load, the size of the cohesive zone and the magnitude of the cohesive traction will also change with the load to maintain the nonsingularity of stresses at the crack tip (Eq. (9.5)).

According to the second assumption, the size of the cohesive zone and the distribution of the cohesive traction at the onset of crack growth are independent of applied

load and crack size. That is, d and $g(\eta)$ in Eq. (9.3) at crack initiation are material properties. Thus, the parameter B should remain constant during crack extension. This constant value can be regarded as a material constant and can be rewritten as

$$B = B_c = \sqrt{\frac{2}{\pi}} \int_0^{d_c} \frac{g_c(\eta) d\eta}{\sqrt{\eta}} \tag{9.6}$$

where $g_c(\eta)$ and d_c are the cohesive traction distribution and the cohesive zone size at the onset of crack growth. In view of Eq. (9.5), the fracture criterion in terms of B_c according to the Barenblatt model is equivalent to Irwin's LEFM criterion in terms of K_{Ic}.

In the Barenblatt model, the specific form of the cohesive traction distribution is not given. Rather, the cohesive traction is related to the separation of atomic layers. A fundamental question arises as to how the cohesive traction on the order of the theoretical strength can be incorporated into an elastic continuum. The Barenblatt model avoids the stress singularity at the crack tip, but creates another problem in linking different scales (atomic to continuum).

It is noted that in the Barenblatt model, the cohesive zone represents a small part of the crack surfaces behind the crack tip, which is in contrast with the currently prevailing concept that the cohesive zone actually represents the fracture process ahead of the crack.

9.2 COHESIVE ZONE CONCEPT IN CONTINUUM MECHANICS AND COHESIVE LAWS

Since the Barenblatt model was introduced, use of the cohesive zone model to treat fracture problems has gained much attention. Besides providing a more realistic feature in fracture mechanism, this model also renders simplicity in simulations of complex cracking processes. From the continuum mechanics point of view, crack extension embodies complex failure processes at the microscopic level, for example, void nucleation, growth and coalescence in ductile metals, microcracking in ceramics, crazing in certain polymers, and so on.

If the failure process is confined in a narrow band, such as crazing in polymers (see Figure 9.2(a)) and necking in ductile thin-sheet materials (see Figure 9.2(b)), the cohesive zone may be used to represent the narrow deformation band. If such a distinct narrow deformation band is not present, the cohesive zone can only be regarded as a hypothesis or an approximate representation of the crack tip failure process zone, such as microcracking in brittle materials (see Figure 9.3(a)) and void growth and coalescence in ductile metals (see Figure 9.3(b)).

In general, it is assumed in the cohesive zone approach that, ahead of the physical crack tip, there exists a cohesive zone, which consists of upper and lower surfaces called cohesive surfaces held by the cohesive traction. The cohesive traction is related

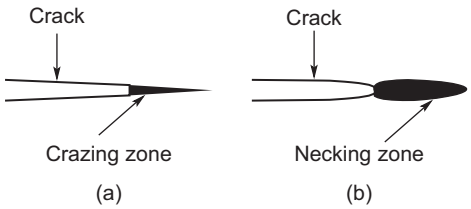

FIGURE 9.2

(a) Crazing zone ahead of a crack in a polymer, (b) necking zone in a ductile thin-sheet material.

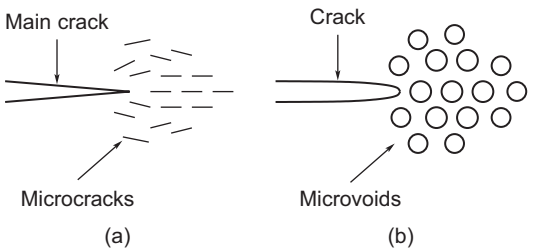

FIGURE 9.3

(a) Microcracking zone ahead of a crack in a brittle solid, (b) voids in a ductile metal.

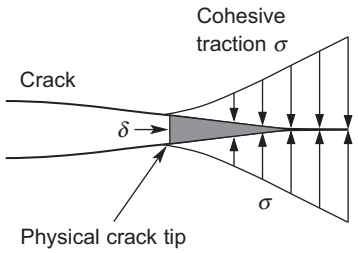

FIGURE 9.4

A cohesive zone ahead of a crack tip.

to the separation displacement between the cohesive surfaces by a "cohesive law." Upon the application of external loads to the cracked body, the two cohesive surfaces separate gradually, leading to physical crack growth when the separation of these surfaces at the tail of the cohesive zone (physical crack tip) reaches a critical value. Figure 9.4 depicts a cohesive zone ahead of a crack where σ is the cohesive traction and δ is the separation displacement of the cohesive surfaces.

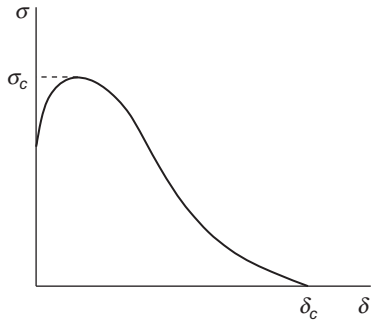

FIGURE 9.5

A general cohesive law describing the relationship between the cohesive traction and the separation displacement.

A cohesive law describes the relationship between the cohesive traction and the separation displacement as follows:

$$\sigma = \sigma_c f(\delta/\delta_c) \tag{9.7}$$

where σ_c is the peak cohesive traction, δ_c a characteristic separation, and f a dimensionless function describing the "shape" of the cohesive traction-separation curve (cohesive curve). The function f depends on the failure mechanism operative either at the microscopic or macroscopic level. Figure 9.5 shows the schematic of the cohesive law Eq. (9.7).

Besides the cohesive parameters σ_c and δ_c, we often use the cohesive energy density Γ_c, or the work of separation per unit area of cohesive surface, defined by

$$\Gamma_c = \int_0^{\delta_c} \sigma(\delta) d\delta \tag{9.8}$$

The cohesive energy density is just the area under the cohesive curve. Once the shape of the cohesive curve is given, only two of the parameters σ_c, δ_c, and Γ_c are independent. When a cohesive zone is based on a distinct narrow deformation band, the cohesive law may be developed by considering the stress and deformation states in the narrow band. For example, Jin and Sun [9-2] derived a cohesive law based on crack front necking in ductile thin-sheet materials. Otherwise, a phenomenological cohesive law is often used. In this case, the cohesive zone parameters such as peak cohesive traction and cohesive energy density need to be calibrated by experiment. Some commonly used phenomenological cohesive laws are given next.

9.2.1 The Dugdale Model

The Dugdale model discussed in Chapter 6 for ductile metals may be regarded as a cohesive zone model. The strip plastic zone is now the cohesive zone and the yield stress is the cohesive traction. The cohesive law is thus given by (see Figure 9.6(a))

$$\sigma = \sigma_c \tag{9.9}$$

Since the cohesive traction is a constant, we need to specify a critical separation displacement, or a cohesive energy density. The relation between them is

$$\Gamma_c = \sigma_c \delta_c \tag{9.10}$$

In using the Dugdale model to simulate fracture propagation, complete separation of materials occurs when $\delta = \delta_c$.

9.2.2 A Linear Softening Model

A linear softening cohesive zone model is often used to describe the progressive failure in some quasibrittle materials, for example, ceramics and concrete. This cohesive law is expressed in the form (see Figure 9.6(b))

$$\sigma = \sigma_c (1 - \delta/\delta_c) \tag{9.11}$$

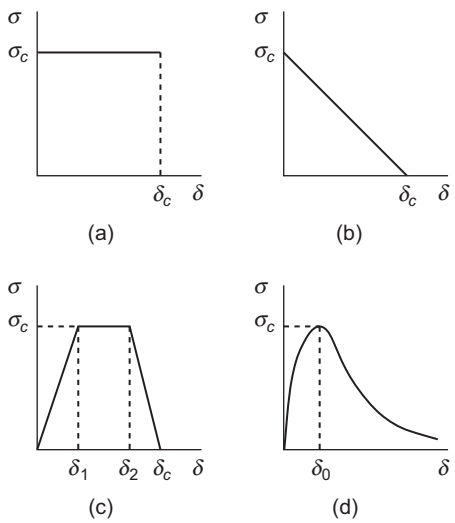

FIGURE 9.6

Cohesive zone models: (a) the Dugdale model, (b) a linear softening model, (c) a trapezoidal model, and (d) an exponential model.

The cohesive energy density is

$$\Gamma_c = \frac{1}{2}\sigma_c \delta_c \tag{9.12}$$

The cohesive law Eq. (9.11) shows that the cohesive traction attains an initial peak value σ_c, decreases with increasing separation displacement, and vanishes at the critical separation of δ_c.

9.2.3 A Trapezoidal Model

The trapezoidal model is an extension of the Dugdale model Eq. (9.9) and the linear softening model Eq. (9.11) with the following traction-separation relationship (Figure 9.6(c)):

$$\sigma = \begin{cases} \sigma_c\,(\delta/\delta_1)\,, & 0 \le \delta \le \delta_1 \\ \sigma_c, & \delta_1 \le \delta \le \delta_2 \\ \sigma_c(\delta_c - \delta)/(\delta_c - \delta_2), & \delta_2 \le \delta \le \delta_c \end{cases} \tag{9.13}$$

where δ_1 and δ_2 are two parameters. The cohesive law Eq. (9.13) can represent a Dugdale model ($\delta_1 = 0$ and $\delta_2 = \delta_c$), a linear softening model ($\delta_1 = \delta_2 = 0$), and their combinations by appropriately selecting the parameters δ_1 and δ_2. The cohesive energy density Γ_c is now given by

$$\Gamma_c = \frac{1}{2}\sigma_c(\delta_c + \delta_2 - \delta_1) \tag{9.14}$$

The cohesive law given in Eq. (9.13), however, is not directly derived from a failure mechanism.

9.2.4 An Exponential Model

An exponential cohesive zone model based on the universal binding energy curve from the atomistic consideration (Rose et al. [9-3]) has found frequent usage in simulating crack growth in ductile metals. The model takes a computationally convenient exponential form (see Figure 9.6(d)),

$$\sigma = \sigma_c \left(\frac{\delta}{\delta_0}\right) \exp\left(1 - \frac{\delta}{\delta_0}\right) \tag{9.15}$$

where δ_0 is the separation displacement at which $\sigma = \sigma_c$, the peak cohesive traction. The cohesive energy density of model Eq. (9.15) is

$$\Gamma_c = \int_0^\infty \sigma\, d\delta = e\sigma_c\delta_0 \tag{9.16}$$

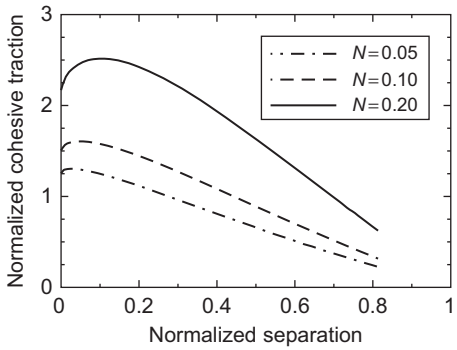

FIGURE 9.7

A cohesive law based on necking (adapted from Jin and Sun [9-2]).

where $e = \exp(1)$. Theoretically, this cohesive energy can be completely dissipated only when the separation displacement becomes unbounded. Practically, the complete separation is assumed to occur when the separation displacement becomes sufficiently larger than δ_0, say, $6\delta_0$. At this point, the cohesive energy dissipated is greater than 95% of Γ_c, and the cohesive traction is less than 5% of the peak value σ_c.

9.2.5 A Cohesive Zone Model Based on Necking

Based on the crack front necking phenomenon in ductile thin-sheet materials [9-4], Jin and Sun [9-2] derived an implicit relationship between the cohesive traction and separation displacement. Figure 9.7 shows the numerical results of the cohesive law for different values of the (power law) hardening exponent N. The cohesive traction is normalized by the yield stress and the separation is normalized by the sheet thickness. It can be seen from the figure that the cohesive traction first increases from a nonzero finite value at the beginning of separation, quickly reaches the peak, and then decreases with further increasing separation displacement. The peak cohesive traction varies from 1.15 times the yield stress for perfectly plastic materials to about 2.5 times the yield stress for modest hardening materials (hardening exponent of 0.2).

9.3 A DISCUSSION ON THE LINEAR HARDENING LAW

The linear hardening traction—separation relationship is a basic element in several widely used cohesive laws. For example, the trapezoidal model Eq. (9.13) reduces to the linear hardening model when the opening displacement of the cohesive surfaces has not reached δ_1. In numerical simulations, a linear hardening model is usually used

as the first step in the nonlinear exponential model Eq. (9.15). The linear hardening model itself has also been used in some studies. These kind of models have a common feature that the cohesive traction takes a zero value at the start of cohesive surface separation (zero separation).

In other words, these models have an initial (or asymptotically initial) linear elastic response. Physically speaking, a cohesive zone model describes the fracture process in a material and the material separation occurs only after it deforms significantly. It is thus expected that cohesive models should have a finite traction at the start of separation, or an initial rigid response. Jin and Sun [9-2] studied the problem from the viewpoint of stress singularity cancellation at the cohesive zone tip.

Consider a two-dimensional elastic medium of infinite extent with a crack of length $2a$ subjected to remote tension p, as shown in Figure 9.8. A cohesive zone of length $\rho = c - a$ develops ahead of each crack tip upon external loading. It is assumed that the cohesive traction σ and the separation δ follow the linear hardening model,

$$\sigma = \begin{cases} \sigma_c\,(\delta/\delta_c)\,, & 0 \le \delta \le \delta_c \\ 0, & \delta > \delta_c \end{cases} \tag{9.17}$$

The cohesive zone modeling approach employs the cohesive crack assumption that the cohesive zone is treated as an extended part of the crack, with the total stress intensity factor vanishing at the tip of the cohesive zone. The stress intensity factor due to the applied load p is

$$K_I^{app} = p\sqrt{\pi c}$$

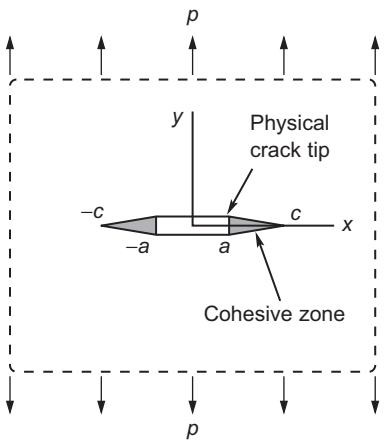

FIGURE 9.8

Cohesive zones ahead of a crack in an infinite elastic solid.

and the stress intensity factor due to the cohesive traction σ may be obtained using the superposition method and the basic solution described in Chapter 3 as follows:

$$K_I^{coh} = -\frac{2}{\sqrt{\pi c}} \int_a^c \frac{\sigma(\xi) d\xi}{\sqrt{1-\xi^2/c^2}}$$

To remove the stress singularity at the cohesive zone tip ($x = c$), we have

$$K_I^{app} + K_I^{coh} = p\sqrt{\pi c} - \frac{2}{\sqrt{\pi c}} \int_a^c \frac{\sigma(\xi) d\xi}{\sqrt{1-\xi^2/c^2}} = 0 \tag{9.18}$$

At the same time, the crack/cohesive surface opening displacement δ is

$$\delta(x) = \frac{4cp}{E^*} \sqrt{1-\frac{x^2}{c^2}} - \frac{4}{\pi E^*} \int_a^c G(x,\xi)\sigma(\xi) d\xi \tag{9.19}$$

where the first and second terms on the right side are due to the external load p and the cohesive traction σ, respectively, $E^* = E$ for plane stress and $E^* = E/(1-\nu^2)$ for plane strain, and $G(x,\xi)$ is a function given by

$$G(x,\xi) = \ln \left| \frac{\sqrt{1-x^2/c^2} + \sqrt{1-\xi^2/c^2}}{\sqrt{1-x^2/c^2} - \sqrt{1-\xi^2/c^2}} \right| \tag{9.20}$$

Substitution of model Eq. (9.17) into Eq. (9.19) and use of Eq. (9.18) lead to the integral equation for the opening displacement δ:

$$\delta(x) + \frac{4\sigma_c}{\pi E^* \delta_c} \int_a^c K(x,\xi)\delta(\xi) d\xi = 0, \quad a \le x \le c \tag{9.21}$$

where $K(x,\xi)$ is the kernel given by

$$K(x,\xi) = G(x,\xi) - 2\sqrt{\frac{1-x^2/c^2}{1-\xi^2/c^2}}, \quad a \le x,\xi \le c$$

Equation (9.21) is a homogeneous linear integral equation for δ and has only a trivial solution. To prove this, we add a nonhomogeneous term,

$$\frac{4cK_{Ic}}{E^*\sqrt{\pi c}} \sqrt{1-\left(\frac{x}{c}\right)^2}$$

to the right side of Eq. (9.21) (where K_{Ic} is a positive constant) to obtain the following equation:

$$\delta(x) + \frac{4\sigma_c}{\pi E^* \delta_c} \int_a^c K(x,\xi)\delta(\xi)d\xi = \frac{4cK_{Ic}}{E^*\sqrt{\pi c}} \sqrt{1 - \left(\frac{x}{c}\right)^2}, \quad a \le x \le c$$

This equation is the integral equation for a crack partially bridged by linear springs. For a general set of cohesive and elasticity parameters $(\sigma_c, \delta_c, E^*)$, the problem has a unique nontrivial solution according to the elasticity theory (Rose [9-5]). This, in turn, requires that its homogeneous equation (9.21) have only a trivial solution [9-6]. The nonexistence of a nontrivial solution for Eq. (9.21) implies that the crack tip singularity can not be canceled. As a result, the cohesive zone model can not assume a linear hardening law with an initial zero cohesive traction, if the stress singularity is to be removed, or if the energy dissipation is not allowed, at the tip of the cohesive zone.

Although the preceding discussion is limited to an infinite plate with a central crack, the conclusion should apply to the general geometric cases and should also apply to the trapezoidal model Eq. (9.13) as well as nonlinear cohesive zone models with $\sigma = 0$ at $\delta = 0$ because the initial nonlinear hardening can be approximated by a linear hardening relationship near $(\sigma, \delta) = (0, 0)$. These kind of nonlinear models include the widely used model Eq. (9.15).

Because the stress singularity can not be removed with a cohesive zone model having an initial linear elastic response, the cohesive zone will not be able to develop naturally, but has to be given a priori. Jin and Sun [9-7] examined the energy dissipation at the tip of a prescribed cohesive zone using a bilinear model ($\delta_1 = \delta_2$ in Figure 9.6(c)). They concluded that the energy dissipation at the cohesive zone tip may be neglected only when the initial stiffness of the cohesive model is appropriately high and the pre-embedded cohesive zone is set much greater than the cohesive zone size with canceled stress singularity at the cohesive zone tip.

9.4 COHESIVE ZONE MODELING AND LEFM

To a certain extent, it is true that the cohesive zone fracture model was introduced partially to remove the stress singularity in the classical continuum crack model and partially to incorporate the physically more realistic material separation mechanisms at the atomic scale. The relation between these two different fracture models is certainly a topic of interest.

We discuss the relationship using the J-integral approach proposed by Rice [9-8]. Consider a cohesive zone ahead of the crack tip as shown in Figure 9.9. Assume that the cohesive zone is so small that the K-field near the crack tip is not disturbed. Evaluating the J-integral along a contour Γ_1 completely embedded in the K-dominance

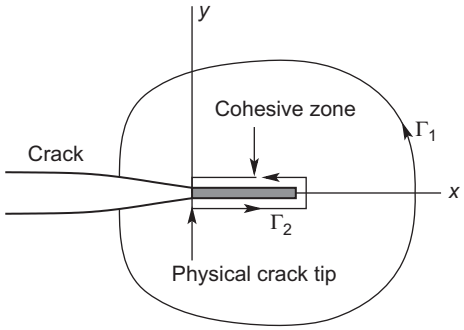

FIGURE 9.9

Integration contours around a crack tip with a cohesive zone.

zone at the (physical) crack initiation state, we have

$$J^{(1)} = \frac{K_{Ic}^2}{E^*} = G_{Ic} \tag{9.22}$$

where K_{Ic} is the fracture toughness and G_{Ic} is the critical energy release rate in LEFM. Alternatively, we may evaluate the J-integral along a contour Γ_2 that consists of the upper and lower surfaces of the cohesive zone. Since $dy = 0$ along the integration path, the J-integral becomes, at the crack initiation state,

$$J^{(2)} = -\int_{\Gamma_2} \sigma_{ij} n_j \frac{\partial u_i}{\partial x_1} dl = -\int_0^{L_c} \sigma(\delta) \frac{d\delta}{dx} dx$$

where L_c is the cohesive zone length at crack initiation. Noting that $\delta = 0$ at the tip of the cohesive zone and $\delta = \delta_c$ at the physical crack tip at crack initiation, the equation can be reduced to

$$J^{(2)} = \int_0^{\delta_c} \sigma(\delta) d\delta = \Gamma_c \tag{9.23}$$

Because no field singularities or discontinuities exist between the contours Γ_1 and Γ_2, the J-integrals evaluated along the two contours should be equal, that is,

$$\Gamma_c = \frac{K_{Ic}^2}{E^*} = G_{Ic} \tag{9.24}$$

This relationship indicates that the cohesive zone model and the LEFM are equivalent when the cohesive energy density is identified as the critical energy release rate in the LEFM and the cohesive zone is embeded in the K-dominance zone.

9.5 COHESIVE ZONE MODELING OF INTERFACIAL FRACTURE

From a physical point of view, the cohesive zone approach appears particularly appropriate for investigating interface fracture because the interface region may be modeled as a cohesive zone. There are, however, a few conceptual issues that need to be examined carefully. For example, the cohesive zone length for Mode I fracture can be determined from the condition that no stress singularities exist at the cohesive zone tip. For interface fracture, however, there are generally two independent cohesive tractions (normal and shear) and a single cohesive zone length may not be able to satisfy the condition that stress singularity at the cohesive zone tip be canceled. It is known from Chapter 8 that interfacial fracture toughness is not a constant but is a function of mode mixity. Such a characteristic of interfacial cracks must also be accounted for by the cohesive zone model. These issues are discussed in this section.

9.5.1 Mixed Mode Cohesive Law

It is known from Chapter 8 that the opening and sliding modes are inherently coupled together in fracture along bimaterial interfaces due to material property asymmetry. When using cohesive zone models to study interface fracture, mixed mode cohesive traction—separation relations are thus required. For mixed opening/sliding mode fracture, there are two separation components across the cohesive surfaces: the opening separation δ_n and the sliding component δ_s. An extension of Eq. (9.7) to the mixed mode cohesive zone model takes the following general form:

$$\begin{aligned} \sigma_n &= f_n(\delta_n, \delta_s) \\ \sigma_s &= f_s(\delta_n, \delta_s) \end{aligned} \tag{9.25}$$

where σ_n and σ_s are the normal and shear cohesive tractions, respectively.

The functional forms of f_n and f_s in Eq. (9.25), or the shapes of the cohesive curves, have not been well understood largely due to the opening/sliding coupling effects. A cohesive energy potential is often used to simplify the procedure of determining f_n and f_s. For example, Needleman [9-9] assumed the existence of a cohesive energy potential $\Phi(\delta_n, \delta_s)$ as a function of two separations δ_n and δ_s and derived the mixed mode cohesive law as follows:

$$\begin{aligned} \sigma_n &= \frac{\partial \Phi(\delta_n, \delta_s)}{\partial \delta_n} \\ \sigma_s &= \frac{\partial \Phi(\delta_n, \delta_s)}{\partial \delta_s} \end{aligned} \tag{9.26}$$

Ortiz and Pandolfi [9-10] defined an effective cohesive traction σ_{eff} and an effective separation δ_{eff}

$$\begin{aligned} \sigma_{eff} &= \sqrt{\sigma_n^2 + \eta^{-2}\sigma_s^2} \\ \delta_{eff} &= \sqrt{\delta_n^2 + \eta^2 \delta_s^2} \end{aligned} \tag{9.27}$$

where η is a coefficient, and assumed that the cohesive energy potential $\Phi(\delta_{eff})$ is a function of the effective separation δ_{eff}. The effective cohesive traction is then derived from the potential $\Phi(\delta_{eff})$ by

$$\sigma_{eff} = \frac{d\Phi(\delta_{eff})}{d\delta_{eff}} \tag{9.28}$$

and the cohesive tractions can be obtained as

$$\begin{aligned} \sigma_n &= \frac{\partial \Phi}{\partial \delta_n} = \frac{d\Phi}{d\delta_{eff}} \frac{\partial \delta_{eff}}{\partial \delta_n} = \frac{\sigma_{eff}}{\delta_{eff}} \delta_n \\ \sigma_s &= \frac{\partial \Phi}{\partial \delta_s} = \frac{d\Phi}{d\delta_{eff}} \frac{\partial \delta_{eff}}{\partial \delta_s} = \eta^2 \frac{\sigma_{eff}}{\delta_{eff}} \delta_s \end{aligned} \tag{9.29}$$

It follows from this equation that $\sigma_n/\sigma_s = \eta^{-2}\delta_n/\delta_s$ which implies a kind of proportional deformation. Tvergaard and Hutchinson [9-11] used a different form of the effective separation and their cohesive traction–separation relations are similar to those in Eq. (9.29).

In general, the cohesive energy density can be calculated from

$$\Gamma_c = \int_0^{\delta_n^c} \sigma_n d\delta_n + \int_0^{\delta_s^c} \sigma_s d\delta_s \tag{9.30}$$

where δ_n^c and δ_s^c are the critical separations at which σ_n and σ_s drop to zero, respectively. In the model of Ortiz and Pandolfi [9-10], the cohesive energy density takes the form

$$\Gamma_c = \int_0^{\delta_{eff}^c} \sigma_{eff} d\delta_{eff} \tag{9.31}$$

where δ_{eff}^c is the effective critical separation corresponding to vanishing effective cohesive traction.

9.5.2 Cohesive Energy Density

The cohesive energy density is a constant for Mode I fracture. For fracture of bimaterial interfaces, however, the cohesive energy density may depend on the loading phase angle. Consider a crack with a cohesive zone at the interface between two dissimilar elastic materials with the shear modulus and Poisson's ratio for the upper and lower media denoted by μ_i and ν_i (i =1,2), respectively, as shown in Figure 9.10.

The J-integral is still path-independent for contours surrounding the crack tip. Consider two integration paths with one (Γ_2) along the boundary of the cohesive zone and the other (Γ_1) within the dominance zone of the elastic oscillatory field

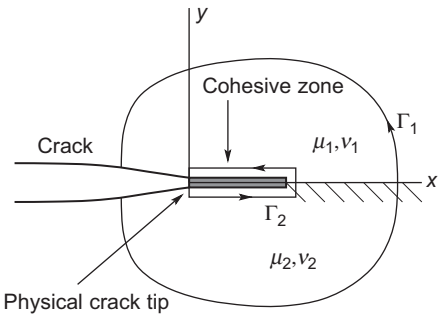

FIGURE 9.10

Integration contours around the tip of an interface crack with a cohesive zone.

(see Eqs. (8.12) and (8.13) in Chapter 8). The J-integral along Γ_1 at crack initiation is evaluated as

$$J = \frac{1}{16}\left(\frac{\kappa_1 + 1}{\mu_1} + \frac{\kappa_1 + 1}{\mu_1}\right)\left(K_1^2 + K_2^2\right) = G_c$$

where G_c is the critical energy release rate. Along path Γ_2 at crack initiation, the J-integral can be evaluated as

$$J = -\int_{\Gamma_2} \sigma_{ij} n_j \frac{\partial u_i}{\partial x_1} dl = -\int_0^{L_c} \sigma_s \frac{d\delta_s}{dx} dx - \int_0^{L_c} \sigma_n \frac{d\delta_n}{dx} dx$$

$$= \int_0^{\delta_n^c} \sigma_n d\delta_n + \int_0^{\delta_s^c} \sigma_s d\delta_s = \Gamma_c$$

It follows from the path-independence of J that

$$\Gamma_c = G_c$$

Here it is assumed that both opening and sliding separations reach their critical values at the physical crack tip at crack initiation.

It is known from Chapter 8 that G_c depends on the phase angle for interface fracture. Hence, the cohesive energy density for interface fracture also depends on the phase angle, that is,

$$\Gamma_c = \Gamma_c(\psi)$$

where ψ is an appropriately defined phase angle, for example, in Eq. (8.62) in Chapter 8.

Consider the special case of $\beta = 0$ for which Mode I and Mode II deformations are uncoupled, where β is the Dundurs parameter defined in Chapter 8. In the phenomenological theory of interface fracture, the critical energy release rate G_c may be expressed as

$$G_c = G_{Ic}\left\{1 + \widetilde{G}(\psi,\lambda)\right\}$$

where G_{Ic} is the critical energy release rate for Mode I fracture and $\widetilde{G}(\psi,\lambda)$ is a dimensionless function of ψ and λ with λ being a free parameter calibrated by experiments. We thus have

$$\Gamma_c = G_{Ic}\left\{1 + \widetilde{G}(\psi,\lambda)\right\} \tag{9.32}$$

The commonly adopted functional forms of $\widetilde{G}$ include [9-12]

$$\widetilde{G}(\psi,\lambda) = \frac{(1-\lambda)\sin^2\psi}{1-(1-\lambda)\sin^2\psi}$$
$$\widetilde{G}(\psi,\lambda) = (1-\lambda)\tan^2\psi$$
$$\widetilde{G}(\psi,\lambda) = \tan^2[(1-\lambda)\psi]$$

We point out that the cohesive energy density consists of its Mode I and Mode II components, which contrasts with the fact that the classical Mode I and Mode II energy release rates of interface fracture do not exist for nonzero oscillation index ϵ as described in Chapter 8.

9.5.3 Cohesive Zone Length

In Mode I fracture, the cohesive zone is determined from the condition that no energy dissipation occurs, or the stress singularity is removed, at the cohesive zone tip. For mixed mode fracture, however, both opening and sliding separations contribute to the energy dissipation. Null energy dissipation at the tip of the cohesive zone thus requires cancellation of singularities in both normal and shear stresses at the cohesive zone tip.

Consider a crack of length $2a$ at the interface between two semi-infinite dissimilar elastic media subjected to remote tension and shear, as shown in Figure 9.11. A cohesive zone of length $\rho = c - a$ develops ahead of each crack tip upon external loading. It is assumed that the cohesive tractions are constant. Consider the small-scale cohesive zone case, that is, $\rho << a$. Hence, $a \approx a + \rho$. The complex stress intensity factor at the cohesive zone tip due to the applied loads is (Eq. (8.27) in Chapter 8)

$$K_{app} = K_1^{app} + iK_2^{app} = \frac{(\sigma_{yy}^{\infty} + i\sigma_{xy}^{\infty})(1+2i\epsilon)}{\cosh(\pi\epsilon)}\sqrt{\pi a} \tag{9.33}$$

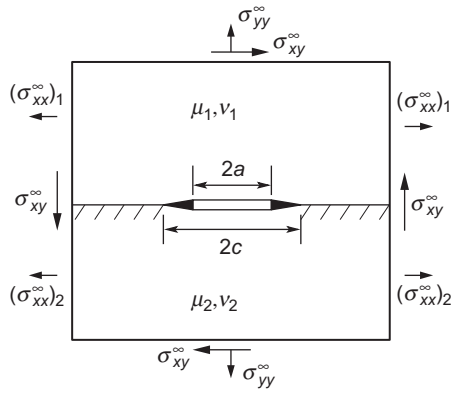

FIGURE 9.11

A crack at the interface between two dissimilar elastic materials.

and the stress intensity factor due to the cohesive traction can be obtained from the Green function solution (Eq. (8.30) in Chapter 8) as

$$K_{coh} = K_1^{coh} + iK_2^{coh} = -\sqrt{\frac{2}{\pi}}(\sigma_n + i\sigma_s)(2a)^{i\epsilon} \int_0^{\rho} \xi^{-1/2-i\epsilon} d\xi$$

$$= -\sqrt{\frac{2}{\pi}}(\sigma_n + i\sigma_s)\left(\frac{2a}{\rho}\right)^{i\epsilon} \frac{2\sqrt{\rho}}{1-2i\epsilon} \tag{9.34}$$

In these two equations, the stress intensity factors have been defined using the same length parameter $2a$ in Eq. (8.36) in Chapter 8.

The cancellation of stress singularity at the cohesive zone tip means

$$K_{app} + K_{coh} = 0 \tag{9.35}$$

or

$$Te^{i\chi} \frac{1+2i\epsilon}{\cosh(\pi\epsilon)} \sqrt{\pi a} = \sqrt{\frac{2}{\pi}} \sigma_0 e^{i\phi} \left(\frac{2a}{\rho}\right)^{i\epsilon} \frac{2\sqrt{\rho}}{1-2i\epsilon} \tag{9.36}$$

where ϕ is the phase angle of the cohesive traction and χ is the loading phase angle, that is,

$$\sigma_n + i\sigma_s = \sigma_0 e^{i\phi}$$

$$\sigma_{yy}^{\infty} + i\sigma_{xy}^{\infty} = Te^{i\chi}$$

Eq. (9.36) contains two independent conditions with only one unknown ρ. It can be satisfied only when

$$\phi = \chi + \epsilon \ln \frac{\rho}{2a} \tag{9.37}$$

It is noted that Huang [9-13] studied the problem in the context of the Dugdale model in which ϕ is determined by Eq. (9.37). It should be pointed out that ϕ in the Dugdale model is determined as the solution of the elastic-plastic boundary value problem and ϕ thus determined may not satisfy Eq. (9.37). As a result, the stress singularity at the Dugdale zone tip may not be canceled. In the cohesive zone model, σ_n and σ_s are assumed to be material-dependent constants. While they may depend on the phase angle χ, Eq. (9.37) can not be satisfied in general, which implies that the stress singularity at the cohesive zone tip may not be canceled.

To deal with this dilemma, Jin and Sun [9-7] proposed a possible remedy that the lengths over which normal and shear tractions act are assumed to be different. For example, if we assume that ρ_n and ρ_s are the lengths of the cohesive zone segments over which normal and shear tractions act, respectively, as shown in Figure 9.12, the stress intensity factor due to the cohesive tractions would be

$$\begin{aligned} K_{coh} &= -\sqrt{\frac{2}{\pi}}(2a)^{i\epsilon}\left[\sigma_n \int_0^{\rho_n} \xi^{-1/2-i\epsilon} d\xi + i\sigma_s \int_0^{\rho_s} \xi^{-1/2-i\epsilon} d\xi\right] \\ &= -\sqrt{\frac{2}{\pi}}\left[\left(\frac{2a}{\rho_n}\right)^{i\epsilon} \frac{2\sigma_n\sqrt{\rho_n}}{1-2i\epsilon} + \left(\frac{2a}{\rho_s}\right)^{i\epsilon} \frac{2\sigma_s\sqrt{\rho_s}}{1-2i\epsilon}\right] \end{aligned}$$

Substituting this equation and Eq. (9.33) into Eq. (9.35) yields the condition for cancelling the stress singularity:

$$\frac{(\sigma_{yy}^{\infty} + i\sigma_{xy}^{\infty})(1+2i\epsilon)}{\cosh(\pi\epsilon)}\sqrt{\pi a} = \sqrt{\frac{2}{\pi}}\left[\left(\frac{2a}{\rho_n}\right)^{i\epsilon} \frac{2\sigma_n\sqrt{\rho_n}}{1-2i\epsilon} + \left(\frac{2a}{\rho_s}\right)^{i\epsilon} \frac{2\sigma_s\sqrt{\rho_s}}{1-2i\epsilon}\right]$$

The equation contains two independent conditions with two unknowns ρ_n and ρ_n. Hence, the stress singularity may be canceled at the cohesive zone tip.

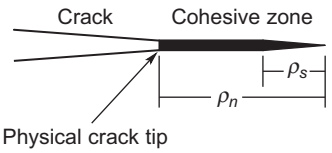

FIGURE 9.12

Different cohesive zone lengths in opening and sliding modes.

References

[9-1] G.I. Barenblatt, The mathematical theory of equilibrium cracks in brittle fracture, in: Advances in Applied Mechanics, Vol. 7, Academic Press, New York, 1962, pp. 55–129.

[9-2] Z.-H. Jin, C.T. Sun, Cohesive fracture model based on necking, Int. J. Fract. 134 (2005) 91–108.

[9-3] J.H. Rose, J. Ferrante, J.R. Smith, Universal binding energy curves for metals and bimetallic interfaces, Phys. Rev. Lett. 47 (1981) 675–678.

[9-4] G.T. Hahn, M.F. Kanninen, A.R. Rosenfield, Ductile crack extension and propagation in steel foil, in: Fracture 1969, Chapman and Hall Ltd., London, 1969, pp. 58–72.

[9-5] L.R.F. Rose, Crack reinforcement by distributed springs, J. Mech. Phys. Sol. 35 (1987) 383–405.

[9-6] R. Courant, D. Hilbert, Methods of Mathematical Physics, Interscience Publishers, New York, 1953.

[9-7] Z.-H. Jin, C.T. Sun, Cohesive zone modeling of interface fracture in elastic bimaterials, Eng. Fract. Mech. 72 (2005) 1805–1817.

[9-8] J.R. Rice, Mathematical analysis in the mechanics of fracture, in: H. Liebowitz (Ed.), Fracture, Vol. 2, Academic Press, New York, 1968, pp. 191–311.

[9-9] A. Needleman, An analysis of tensile decohesion along an interface, J. Mech. Phys. Sol. 38 (1990) 289–324.

[9-10] M. Ortiz, A. Pandolfi, Finite-deformation irreversible cohesive elements for three-dimensional crack-propagation analysis, Int. J. Numer. Methods Eng. 44 (1999) 1267–1282.

[9-11] V. Tvergaard and J.W. Hutchinson, The influence of plasticity on mixed mode interface toughness, J. Mech. Phys. Sol. 41 (1993) 1119–1135.

[9-12] J.W. Hutchinson and Z. Suo, Mixed mode cracking in layered materials, Adv. Appl. Mech. 29 (1992) 63–187.

[9-13] N.C. Huang, An estimation of the plastic zone size for a bimaterial interfacial crack, Eng. Fract. Mech. 41 (1992) 935–938.

PROBLEMS

9.1 Prove that the cohesive energy densities for the trapezoidal model Eq. (9.13) and the exponential model Eq. (9.15) are given by Eq. (9.14) and (9.16), respectively.

9.2 Find the relation between the critical separation displacements δ_c in the linear softening model Eq. (9.11) and δ_0 in the exponential model Eq. (9.15), assuming identical peak cohesive traction σ_c and identical cohesive energy density Γ_c in the two models.

9.3 Derive the integral expression of the cohesive energy density Eq. (9.31) from Eq. (9.30). Assume that the opening, sliding, and effective separations reach their critical values δ_n^c, δ_s^c, and δ_{eff}^c simultaneously.